Article

Surfactant Provided Control of Crystallization Polymorphic Outcome and Stabilization of Metastable Polymorphs of 2,6-Dimethoxyphenylboronic Acid

Aina Semjonova * and Agris Bērziņš

Faculty of Chemistry, University of Latvia, Jelgavas iela 1, LV-1004 Rīga, Latvia
* Correspondence: aina.semjonova@lu.lv

Abstract: 2,6-Dimethoxyphenylboronic acid was used as a model substance to investigate the additive crystallization approach for polymorph control in phenylboronic acids. It was crystallized under different conditions by performing evaporation and cooling crystallization from different solvents. Most of the crystallizations from pure solvents produced the thermodynamically stable Form I, but in evaporation crystallization from alcohols, Form II or even a new polymorph, Form III, could be obtained. Structurally related substances, polymers, and surfactants with diverse intermolecular interaction possibilities were tested as additives. Surfactants were found to facilitate the crystallization of the metastable forms and therefore were investigated more extensively. The surfactants Span 20 and *n*–octyl-β-D-glucopyranoside provided crystallization of the metastable forms in the evaporation crystallization and notably stabilized Form II. The lattice energy, energy frameworks, Hirshfeld surface analysis, full interaction maps, and morphology prediction were used to identify the structural differences between Forms I and II and rationalize the ability of the additives to provide formation of Form II in the crystallization and to stabilize it.

Keywords: 2,6-Dimethoxyphenylboronic acid; polymorphism; crystallization; crystallization additives; crystal structure analysis

1. Introduction

Most of the drug dosage forms of active pharmaceutical ingredients (APIs) are in solid form. These drug dosage forms include not only tablets and capsules, but also powders for parenteral applications and powder inhalers [1]. Approximately half of APIs show the ability to crystallize in different polymorphs [1,2]. Polymorphs have the same chemical composition but different molecule packing and/or conformation in the crystal lattice [3,4]. They have different physical properties—for example, solubility [5,6], bioavailability [7] or sometimes colour [8]. It is important to perform polymorph screening and identify the stable polymorph before drug manufacturing [1,4]. In addition, it is required to check the stability of the selected polymorph in long-term storage. There have been several cases [9] where a new and more stable polymorph appeared many years after drug development. Such late appearance of a more stable polymorph can cause problems for patients, from low drug efficacy to eventually disrupting the supply of medicines [10]. Metastable polymorphs, although having better solubility and dissolution rates [4], can transform to the stable form [6]. Therefore, there is a need to improve the stability of metastable forms. One way to achieve this is to inhibit the transformation rate by using additives in the crystallization process or in the drug dosage form. Additives usually improve the kinetic stability of the metastable form [11] but can also change the relative stability of polymorphs [12,13]. The effect of additives on nucleation has been extensively studied [14], but there is still too little evidence for understanding the mechanism of additive provided crystallization polymorphic outcome control. Additives can affect the kinetics of nucleation and related parameters [14–18], the thermodynamic aspects of crystallization, or both of these aspects

simultaneously [11]. Additive crystallization is widely used in natural and industrial processes, from biomineralization to material synthesis [19].

It is known that crystals containing similar hydrogen bond synthons can epitaxially grow on structurally related additives [20]. Structurally similar additives can inhibit [21] or promote [15,22–25] nucleation of a specific polymorph. Nucleation inhibition can occur by blocking the movement of surface steps, kinks, or terraces, therefore inhibiting crystal growth [18]. On the contrary, small, structurally similar molecular compounds can also be integrated into the lattice and operate as a pre-nucleation precursor [11,18] but will lead to this additive being an impurity of the obtained crystals. According to the European Pharmacopoeia, it is important to identify impurities to ensure the safety of pharmaceutical products [26], and structurally related additives can have a pharmacological or toxic effect [27–30]. Therefore, not all structurally related additives can be used to stabilize the polymorphic form in pharmaceutical formulations.

In contrast, many surfactants and polymers can be used in drug dosage forms [31,32]. Polymers are often used as tablet binders, for film formation, as taste-maskers, drug-release controllers, thickeners, etc. [31], but surfactants can be used in suspensions, emulsions, gels, or drug delivery systems as drug protectors (e.g., nanoparticles or liposomes in drug dosage forms) [32]. This is an advantage of these additives compared to the structurally related additives. Some polymers, such as polyethylene glycol, polystyrene, and poly-methylmethacrylate, can decrease surface tension and act as a surfactant [33]. As surface tension and nucleation rates are inversely related, surfactants decrease surface tension and can promote nucleation of the metastable form [11]. Surfactants can decelerate phase transitions [19,34] by increasing the activation barrier for nucleation of the stable form [19]. Surfactants can also increase the solubility and dissolution rate of API by incorporating it into their micelles or hemispheres [11,35]. The hydrophilic part of the surfactant can be strongly attached to the crystal surface, but the hydrophobic chain can cover the crystal surface and prevent other interactions [17]. Larger additives can adsorb on a non-specific crystal surface and therefore inhibit crystal growth by hindering the deposition of growth units [34]. Polymer additives can act as nucleation sites by absorbing into pre-nucleated clusters and therefore reducing interfacial free energy and changing the interactions between the solute molecules [11].

In this study we investigated additive assisted crystallization by focusing on the preparation of a metastable polymorph to obtain a better understanding of the mechanism of additive provided polymorphic outcome control. 2,6-Dimethoxyphenylboronic acid (MPBA), existing as two polymorphs [36], was used as a model compound. Overall, some arylboronic acids are important in the pharmaceutical industry due to their biological activity and the possibility of pharmacological effects [37–42]. MPBA was selected due to the different hydrogen bonding motifs present in both of its polymorphs, including a trimeric motif uncharacteristic of phenylboronic acids. We explored structurally related molecules, polymers, and surfactants with diverse possibilities for intermolecular interaction as additives. To explore additive assisted crystallization of MPBA, we performed polymorph screening, tested which additives allow crystallization of the metastable form, and explored the most promising additives for crystallization of the metastable polymorph by varying the crystallization conditions. To access the mechanism of additive provided crystallization and stabilization of the metastable form, we used crystallographic analysis and theoretical calculations.

2. Materials and Methods

2,6-Dimethoxyphenylboronic acid (MPBA, purity 97%, polymorph I) and *n*-octyl-β-D-glucopyranoside (OGP, purity > 99 %) was purchased from Fluorochem. Span 20 (sorbitan monolaurate) with ≤1.0 % water was purchased from Merck. Molecular structures of MPBA and the most extensively studied additives are shown in Figure 1. The water was deionized in the laboratory. Other additives (see Supplementary Materials, Table S1) and organic solvents of analytical grade were purchased from different commercial sources.
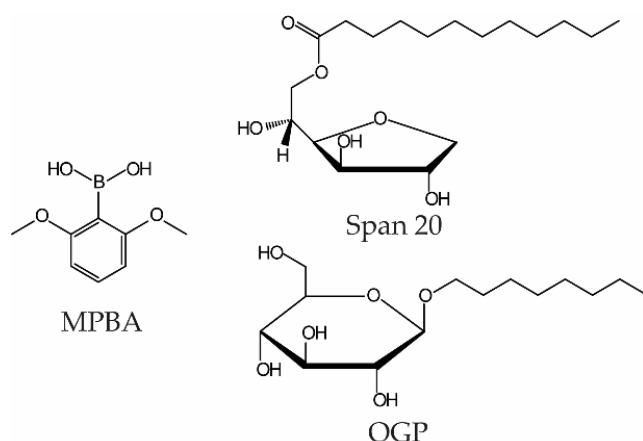
Figure 1. Molecular structure of MPBA, Span 20, and OGP.

2.1. Solubility Measurements

The approximate solubility of MPBA in selected solvents was determined gravimetrically. Saturated solutions of MPBA in water, acetonitrile, toluene, tetrahydrofuran, nitromethane, and isopropanol were prepared at ambient temperature. Solutions (1 or 5 mL) were evaporated at 80 °C, and the mass of residual solid was used for calculation of the solubility. Approximate solubilities of MPBA Form I are listed in Table S2.

2.2. Crystallization Experiments

Commonly used solvents from different solvent classes were selected for the crystallization of MPBA. For evaporation crystallization, 30 to 50 mg of MPBA were dissolved in 2 to 3 mL of solvent and evaporated at 25 or 50 °C. For cooling crystallization, MPBA was dissolved at 40 to 80 °C, depending on the boiling points of the solvent. The obtained solutions were filtered and cooled to 5 °C. The obtained solid products were collected by filtration, air dried, and characterized with powder X-ray diffraction (PXRD).

Cooling crystallizations were also performed using Crystal16 (Technobis Crystallization Systems, Alkmaar, Netherlands). Solutions of different supersaturation ($S = c/c^*$, where c is the initial concentration and c^* is the solubility at 25 °C, for toluene $c/c^* = 2$–11; for water $c/c^* = 5$–10) were prepared in situ (the required mass of MPBA and 1.00 mL of solvent were transferred into the HPLC vial, and dissolution was achieved by heating in Crystal16) and cooled with a cooling rate of 10 °C·min^{-1} by stirring at a rate of 900 rpm. Toluene solutions with $c/c^* = 10$ were cooled with different cooling rates—20, 10, 1, and 0.1 °C·min^{-1}—to determine the effect of the cooling rate on the polymorphic outcome. Water solutions with high supersaturation, obtained using higher temperatures for dissolution or a long cooling time, oiled out and were not used for phase analysis. Four parallel crystallization experiments were performed in all cases. The obtained solid products were collected by filtration, air-dried, and characterized with PXRD.

Crystallization from toluene and water in the presence of additives was performed using cooling. Soluble additives were selected for the crystallization. In 2 mL of water at 70 °C, 20–25 mg of additive and 40–45 mg of MPBA were dissolved, and the solution was filtered and cooled to 5 °C. In 2 mL of toluene at 90 °C, 20–25 mg of additive and 100–110 mg of MPBA were dissolved, then the solution was filtered and cooled to 5 °C. Crystallization from toluene in the presence of surfactants was carried out also using different crystallization methods: complete solvent evaporation at 5, 25, and 50 °C and evaporation crystallization with stirring at 25 °C. For evaporation at 5 and 25 °C, solutions were prepared by dissolving 40–50 mg of MPBA and 100–110 mg of a liquid surfactant or 20–25 mg of a solid surfactant in 3 mL of toluene at 70 °C. The solutions were filtered and kept at the specified temperature for evaporation (no crystal nuclei formed at cooling). For evaporation crystallization at 50 °C solutions were prepared by dissolving 100–110 mg of

MPBA and 230–250 mg of a liquid surfactant or 100–110 mg of a solid surfactant in 2 mL of toluene at 70 °C. The solutions were filtered and kept at 50 °C for evaporation. For cooling crystallization with stirring at 25 °C, solutions were prepared by dissolving 140–150 mg of MPBA and 100–110 mg of a liquid surfactant or 40–50 mg of a solid surfactant in 2 mL of toluene at 70 °C; the solution was then filtered and cooled to 25 °C by stirring the solution at 700 rpm.

Crystallization in the presence of other viscous additives was performed using several crystallization methods—complete solvent evaporation at 25 and 50 °C and cooling crystallization at 5 °C. 100–110 mg of additive and 100–110 mg of MPBA were dissolved in 2 mL of toluene at 90 °C, and the solution was filtered and kept under the specified conditions for crystallization. Crystallization from other solvents in the presence of Span 20 was performed by evaporation crystallization. 100–110 mg of Span 20 and 100–110 mg of MPBA were dissolved in 2 mL of solvent at 40 to 90 °C depending on the boiling point of the solvent. The solution was filtered and placed at 50 °C for evaporation. For each additive, three parallel crystallization experiments were performed. The obtained products were collected by filtration or by scraping from the crystallization container, air-dried, and characterized with PXRD.

2.3. Solid Phase Characterization

The PXRD patterns were measured at ambient temperature on a Bruker D8 Advance (Bruker AXS, Karlsruhe, Germany) diffractometer equipped with a LynxEye position sensitive detector using copper radiation (Cu K_α; λ = 1.54180 Å). Tube voltage and current were set to 40 kV and 40 mA, respectively. The divergence slit was set at 0.6 mm. The anti-scatter slit was set at 8.0 mm. The PXRD patterns were recorded from 3° to 35° on the 2 θ scale. The scan speed of 0.2 s/0.02° was used.

DSC analysis of MPBA polymorphs was performed using a TA DSC 25 (TA Instruments, New Castle, DE, USA) calorimeter. Closed aluminium pans were used. The heating of the samples from 25 to 200 °C was carried out at a heating rate of 10 °C·min^{-1} or 2 °C·min^{-1} for Form II. Samples of 1 mg mass were used. The nitrogen flow rate was 50 mL·min^{-1}. TG analysis was performed using the Mettler Toledo TGA/DSC 2 (Mettler Toledo, Greifensee, Switzerland). Closed aluminium pans were used. The heating of the samples from 25 to 200 °C was carried out at a heating rate of 10 °C·min^{-1}. Samples of 5 to 8 mg mass were used. The nitrogen flow rate was 30 mL·min^{-1}.

2.4. Phenylboronic Acid Derivative CSD Structure Analysis and Theoretical Calculations

Cambridge Structural Database (CSD) version 5.43 [43] was searched to analyse the intermolecular interactions present in phenylboronic acid derivative structures using ConQuest 2022.2.0 [44]. A total of 510 structures with phenylboronic acid fragments were found. Structures containing more than one component, compounds with metal coordinative bonds, and organoboronic compounds not classified as boronic acid were excluded from the analysis. Hydrogen bond interactions were analysed in Mercury 2020.3.0 [45].

Geometry optimization of the crystal structures of both polymorphs was performed in Quantum ESPRESSO 6.4.1 [46] by relaxing the positions of all atoms. The initial geometry of the crystal structures was taken from the CSD database (Form I—UJACIT01; Form II—UJACIT). The crystal structure of Form I was modified to remove the disorder in the boronic acid group appearing because of the symmetry. This was done by reducing the symmetry of the structure to the *P*1 space group and, in several different ways, by removing the redundant hydrogen atoms from the boronic acid groups by obtaining ordered dimers formed by MPBA in *syn-anti*-conformation. Then, among the obtained structures, a monoclinic *Pc* structure with Z′ = 2 was identified as the structure with the highest possible symmetry with the ISOCIF tool (version 3.1.0) [47]. All calculations were performed using the PBE functional with ultrasoft pseudopotentials from the original pseudopotential library and a 90 Ry plane-wave cutoff energy with vdW interactions treated according to the D3 method of Grimme [48] using a 2 × 2 × 2 k-point

grid. Geometry optimized structures were used for further analysis performed using Crystal Explorer 21 [49].

Intramolecular energy was calculated by performing full geometry optimization of the MPBA molecule and geometry optimization with dihedral angle of the boronic acid group constrained to the value as present in the crystal structures of Form I and Form II in the gas phase. Calculations were performed in Gaussian 09 Revision D.01 [50] with the density functional theory M06-2X and 6-31++G(d,p) basis set. Intramolecular energy was calculated as the difference between the energy of the conformer as in the crystal structure and the global minimum energy.

Calculations of pairwise intermolecular interaction energy in crystal structures were performed in CrystalExplorer 21 at the B3LYP-D2/6-31G(d,p) level. The sum of all pairwise interaction energies with molecules for which the atoms are within 15 Å of the central molecule was used to estimate the intermolecular energy. The lattice energy was calculated by summing the intermolecular energy calculated in CrystalExplorer, and intramolecular energy was calculated using Gaussian09 [51].

Hirshfeld surfaces, their 2D fingerprint plots summarizing the information about intermolecular interactions and generation of energy frameworks from the calculated pairwise interaction energies, and their electrostatic and dispersion components were calculated with CrystalExplorer 21.

Generation of Full Interaction Maps (FIM) providing molecule interaction preferences and analysis of Bravais–Friedel–Donnay–Harker (BFDH) morphology [52] were performed with Mercury 2020.3.0. FIMs of individual molecules as well as crystal structures with crystal facets of BFDH morphologies were generated for each polymorph.

3. Results and Discussion

3.1. Crystallization from Pure Solvents

We crystallized MPBA from popular solvents from different solvent classes. In almost all crystallizations, particularly from aprotic solvents, pure Form I was obtained (see Table 1). However, from polar protic solvent (isopropanol, methanol, and isobutanol) it was possible to obtain the metastable MPBA Form II. Besides the already known polymorphs, we also obtained a new MPBA polymorph, designated as Form III (see Figure 2). Form III crystallized together with Form II in evaporation crystallization from isopropanol, isobutanol, and heptanol. For further crystallization studies aimed at identifying which additives would allow crystallization of the metastable forms, we selected water and toluene because of their better suited MPBA solubility (see Supplementary Materials, Table S2), higher boiling point, and crystallization of the stable polymorph I from these solvents (see below).

Table 1. Polymorphic outcome of crystallization from pure solvents.

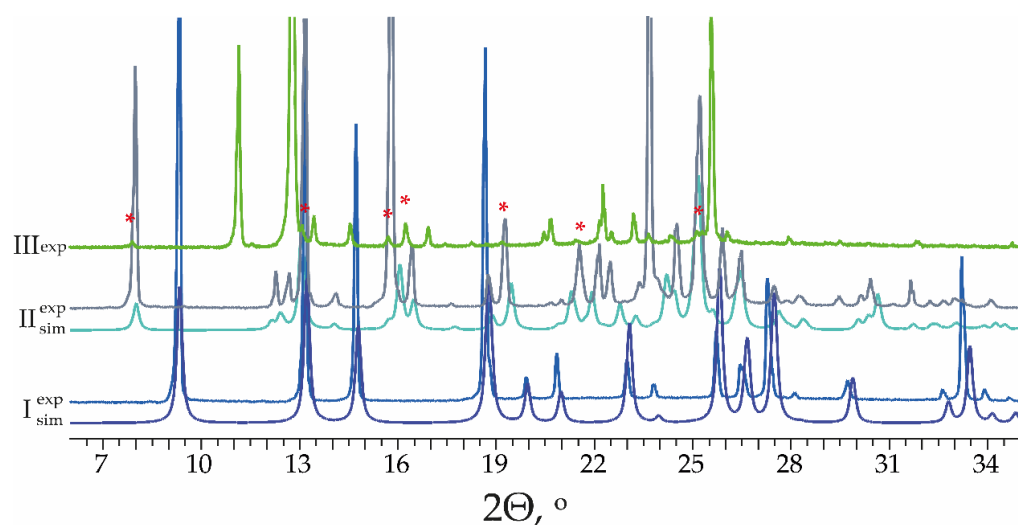| Solvent	Cooling	Evaporation	
		25 °C	50 °C
Acetone; acetonitrile; ethyl acetate; toluene; nitromethane; *o*–xylene; chloroform; 1,4-dioxane; methyl tert-butyl ether; dichloromethane; diethyl carbonate; tetrahydrofuran; methyl isobutyl ketone; cyclohexanol	I	I	I
2,2,2-Trifluorethanol; water	I	I	I + II
Heptanol	I	II + III	I
Isopentanol	I	I + II	I
Isobutanol	I	I + II	II
Isopropanol	I	II/II + III	I + II
Methanol	II	II	I

Figure 2. Simulated and experimental PXRD patterns of MPBA polymorphs. The possible Form II impurity in the Form III sample is marked with red asterisks.

For more thorough characterization of the crystallization of MPBA from water and toluene, we investigated the effect of supersaturation, as it can have a great impact on the polymorphic outcome. Usually, higher supersaturation results in the formation of metastable forms [53–55]. Water solutions with supersaturation ($S = c/c^*$) from 5 to 10 (11–22 mg·mL^{-1}) were crystallized with a cooling rate of 10 °C·min^{-1} and a stirring rate of 900 rpm. Higher supersaturation, heating the solution above 70 °C, or long stirring at an elevated temperature resulted in the solution oiling out. Furthermore, before the nucleation at cooling the solution always oiled out and only then did nucleation occur. Toluene solutions with supersaturation between 2 and 11 (24–132 mg·mL^{-1}) were crystallized under the same conditions, except that solutions with $c/c^* = 10$ were also cooled at different cooling rates, from very fast (20 °C·min^{-1}) to very slow (0.1 °C·min^{-1}). The toluene solutions did not oil out, but in all solutions, solid particles (a few small crystals in the solution) were observed before extensive nucleation, when numerous MPBA crystals appeared and began to grow by forming a suspension. For solutions with lower supersaturation, the solid particle formation point was near 20–30 °C, but more crystals were obtained only when the mixture reached 10 °C and was stirred for 5 to 10 min. When supersaturation was increased, the solid particle formation and nucleation occurred at a higher temperature (for $c/c^* = 10$ it was at ~80 °C and 32–20 °C, respectively). Nevertheless, neither in water nor in toluene did the supersaturation and cooling rate (tested for toluene) affect the polymorphic outcome, as Form I was always obtained in the crystallization. Therefore, we have demonstrated that metastable forms do not crystallize in cooling crystallization from toluene and water under the investigated conditions.

3.2. Characterization of MPBA Polymorphs

3.2.1. Structure Analysis of MPBA Polymorphs and Analysis of Phenylboronic Acid Moiety Interaction Preferences in CSD Structures

MPBA has two known polymorphic forms characterized by Cyrański et al. [36]. Form I crystallizes in the tetragonal crystal system $P\bar{4}n2$ with Z′ = 0.5 and contains typical hydrogen bonded homodimers of boronic acid that adopts *syn-anti*-conformation. Form II crystallizes in the monoclinic crystal system $C2/c$ with Z′ = 1.5 and contains an unusual hydrogen-bonded boronic acid synthon formed by three molecules (see Figure 3). The trimer synthon consists of two symmetry independent molecules in the *anti* conformation—the middle molecule (A) forms hydrogen bonds with terminal molecules (B), which act as hydrogen bond acceptors. Additionally, in the terminal molecules (B), there are two intramolecular hydrogen bonds between the hydroxyl and methoxy groups. As we demonstrate below,

the hydrogen bonding as in Form II is unusual for arylboronic acids. Unfortunately, our attempts to determine the crystal structure of Form III were unsuccessful, as suitable crystals for SCXRD analysis were not obtained and the bulk sample contained an impurity of Form II (see Figure 2).
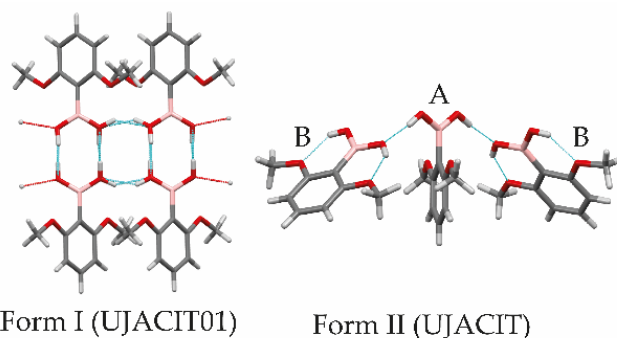

Form I (UJACIT01)　　　　Form II (UJACIT)

Figure 3. Hydrogen bonding in the crystal structures of MPBA polymorphs and labelling of molecules in Form II.

In CSD, 209 crystal structures of single component phenylboronic acid phases (see Supplementary Materials, Figure S1) were found, resulting in analysis of 192 unique crystal structures. The analysis showed that polymorphism in phenylboronic acid is rarely reported in CSD: only 7 of 185 (3.8%) unique compounds have structures of two polymorphs. For five of the phenylboronic acid derivatives, polymorphs have different intermolecular interactions, including dimers, chains, and intramolecular and specific intermolecular hydrogen bonds (see Supplementary Materials, Table S3). Boronic acid homodimers are present in most of the phenylboronic acid structures (82.8%), while only 14.6% of structures have chain-like hydrogen bonding. In two structures (1.0%) there are dimers and chains (see Figure S4), but in three structures (1.6%), only intramolecular hydrogen bonds. The dimers can be divided into six different types (see Supplementary Materials Figure S2 and Table S4) according to the hydrogen bonding in the crystal structure. MPBA Form I contains A1 type dimers (formed by $R_2^2(8)$ dimers connected by 2 mutual C(4) chains), which is common for phenylboronic acids (28.3% of all the dimeric structures). The most abundant phenylboronic acid dimer synthon is type B1 (35.8% of all the dimers), an isolated dimer with additional intramolecular hydrogen bonds.

Other types of hydrogen bond synthons formed by phenylboronic acid moieties are quite different but can be divided into eight types (see Supplementary Materials, Figure S3 and Table S5). The most abundant among these are hydrogen bonds with other atoms in the molecule (35.5% of all non-dimers) (Figure S3, type H). Boronic acid trimers as in Form II (Figure S3, type K) are unique and not observed in any other structure, although there are structures in which there are only intramolecular hydrogen bonds as present in molecule B (9.7%), and two structures (type J) in which there are either different isolated hydrogen bonds with molecules in *anti* conformation or chains C(2) formed by such hydrogen bonds.

Therefore, the performed CSD analysis confirms that dimers are the main hydrogen bond type for phenylboronic acids as suggested before [37,38,56–60] and that MPBA Form II is a unique trimer containing structure. Overall, there is a relatively low possibility for formation of a phenylboronic acid derivative structure not containing dimers, particularly if there are no other functional groups which could lead to disruption of hydrogen bonds formed by only boronic acid moiety. Nevertheless, we believe that the polymorphism of phenylboronic acid derivatives is not thoroughly studied, as suggested by the notably low number of polymorphic molecules. For example, a study by Cruz-Cabeza et al. shows that polymorphism occurrence in single component crystals is at least 37% and more polymorphic structures are reported for more thoroughly studied substances with pharmacology effect [61].

3.2.2. Thermal Characterization of MPBA Polymorphs

Thermal analysis showed that the melting point of Form I is 108 °C (see Figure 4). In DSC analysis of Form II at 2 °C·min^{-1} an exothermic peak corresponding to phase transition to Form I was detected at 74 °C (confirmed by PXRD). This indicates the monotropic relationship between Form I and Form II [62]. The phase transition of Form II to Form I at 80 °C was confirmed by heating in a thermostat for an hour. The newly obtained Form III has a melting peak at 52 °C. As Form III has a lower melting enthalpy and melting point than Form I, these polymorphs are also monotropically related by the heat of fusion rule [62]. When the Form III sample was stored at a 60 °C thermostat, transformation to Form I occurred before the melting. Such a high melting point difference of more than 50 °C between Form I (108 °C) and Form III (52 °C) is rarely observed [63] and indicates low thermodynamic stability of Form III. The absence of mass change in the TG curves (see Supplementary Materials, Figures S5–S7) confirmed that all the obtained phases are polymorphs. We note that Form II and Form III are not stable in ambient conditions: Form II transforms into Form I in <24 h, whereas Form III transforms into Form II in <1 h. In contrast, Form II is stable notably longer at lower temperatures in the freezer.
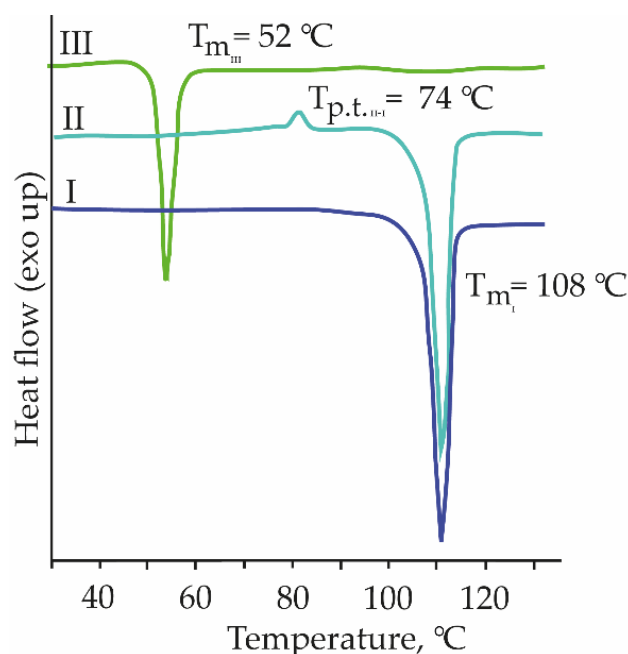

Figure 4. DSC curves of MPBA polymorphs (heating rate 10 °C·min^{-1} for Forms I and III, 2 °C·min^{-1} for Form II). The onset temperatures were used to characterize the thermal process occurring in the DSC traces.

3.3. Crystallization in the Presence of Additives

When crystallizing from water, the hot sample at the beginning of the cooling always oiled out first and crystallized only later. However, the nucleation was very slow, as a solid was obtained after only a few hours or even a few days, and only Form I was obtained by cooling a water solution in the presence of additives.

Overall, polymorph I was obtained in most of the cooling crystallizations of toluene solutions in the presence of additives, in agreement with this polymorph obtained in cooling crystallization of pure solvent (see Supplementary Materials, Figure S8). However, in the presence of octyl β-D-glucopyranoside (OGP) and 2,6-dimethoxybenzoic acid (2,6MeOBA), a mixture of Forms I and II can be obtained. We note that MPBA as an additive promotes the formation of the metastable form of 2,6MeOBA [64]. As the polymorphs of both substances differ by *syn-* and *anti* conformers in the structure, it is possible that the 2,6MeOBA *syn*

conformation stabilizes the MPBA *anti* conformation by forming hydrogen bonds, therefore allowing easier nucleation of Form II.

Serendipitously, we discovered that evaporation of the filtrate obtained in crystallization from toluene in the presence of all the surfactants (OGP, Polysorbate 80, Span 20 and Tween 20) resulted in formation of Form II crystals. Therefore, surfactants were selected for further additive crystallization experiments. Crystallization was performed using two different approaches: cooling and evaporation crystallization. In the cooling crystallization with these additives, almost exclusively Form I was obtained (see Figure 5), whereas the metastable Form II was obtained in only one of the experiments. In contrast, Form II, Form III, or their mixture was obtained in evaporation crystallization in the presence of Span 20, Tween 20, and OGP. We observed that the presence of Span 20 and OGP stabilizes Form II but not Form III, because it very rapidly transformed into Form II as observed by the PXRD analysis. However, Form II was stable for up to one month in the presence of these two surfactants. We also observed that evaporation with stirring prevented crystallization of the metastable forms. Among the tested conditions, the best for obtaining metastable forms was solvent evaporation at 50 °C without stirring. Under these conditions, the presence of Span 20 and OGP in the initial solution resulted in crystallization actually occurring from a MPBA solution in the surfactant after the evaporation of the initial solvent when the obtained mixture was cooled to room temperature. The crystals obtained in this procedure were very small, and pure polymorph III crystallized in the presence of Span 20 and OGP. Nevertheless, single crystals were not obtained, and the presence of the wide peaks of Span 20 and OGP also prevented structure determination from the PXRD data.
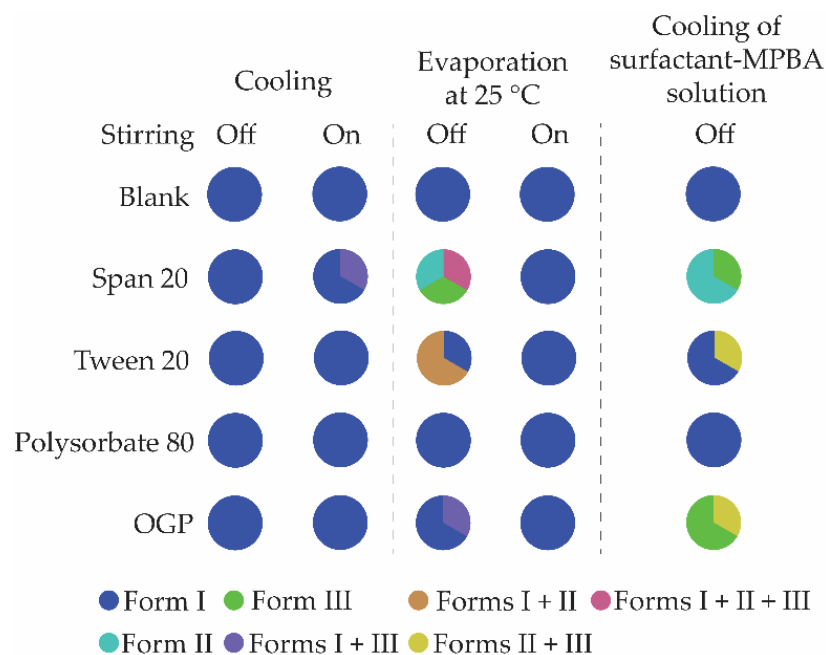

Figure 5. Polymorphic outcome in crystallization from toluene in the presence of surfactants using different crystallization methods. Each third of the circle represents one of the parallel experiments.

MPBA–Span 20 solution was also obtained using other solvents to determine whether the initial solvent has a role if the crystallization is performed in this way. Five solvents were selected: four solvents from which only Form I was previously obtained and isopropanol from which Form II was obtained. A clear MPBA solution in Span 20 later crystallizing at room temperature was obtained after the evaporation of all these solvents. Pure Form II was obtained in all 15 experiments. Therefore, the formation of Form II under these conditions is purely determined by Span 20.

Span 20 and OGP at 50 °C are viscous liquid substances. Therefore, other viscous liquid substances were also examined. Crystallization was performed using cooling crystallization and evaporation crystallization without stirring, as the stirring did not allow for formation of the metastable forms. The results showed that the formation of metastable forms is not provided by any viscous liquid, as among the tested, only PEG 600 showed the potential for crystallization of Form II in evaporation crystallization (see Figure 6). Therefore, the main reason for polymorph control apparently is the intermolecular interactions between the surfactant molecules and the MPBA.
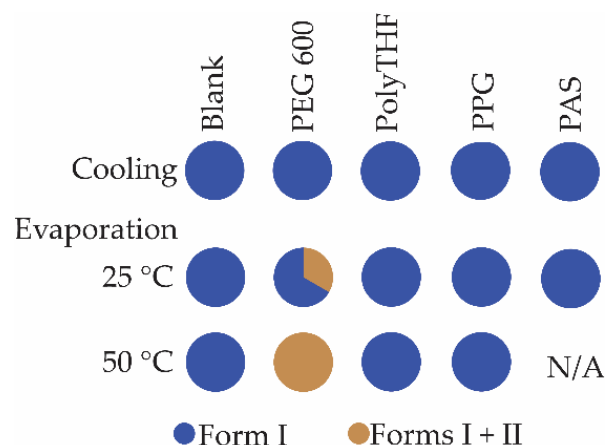

Figure 6. Polymorphic outcome in crystallization from toluene in the presence of viscous liquids as additives using different crystallization methods. Each third of the circle represents one of the parallel experiments. Abbreviations: PEG—polyethylene glycol; PolyTHF—poly tetrahydrofuran; PPG—polypropylene glycol; PAS—poly(acrylic acid).

3.4. Theoretical Analysis of MPBA Crystal Structures

To find the intramolecular energy of MPBA in its crystal structures, two conformers—*syn-anti* and *anti*—were considered. The *anti* conformer with two intramolecular hydrogen bonds between boronic acid hydroxyl groups and methoxy groups (as in B molecule of Form II) was found to be the global energy minimum. The *syn-anti* conformer (similar to conformation in Form I but with the boronic acid group almost in plane with the benzene ring and therefore having one intramolecular hydrogen bond) was found to be less efficient by 12 kJ·mol^{-1} (see Supplementary Materials, Table S6). Not surprisingly, the intramolecular hydrogen bonds in MPBA result in differing energy of conformers compared to those reported in studies of phenylboronic acid in aprotic solvents and in vacuo, where generally the *syn-anti*-conformers are energetically more stable than the *anti* by ~5 kJ·mol^{-1} [65]. The geometry optimizations with constrained torsion angle between the benzene ring and boronic acid group were used to calculate the intramolecular energy of MPBA. These calculations showed that in Form II, the B molecule almost fully corresponds to the global energy minimum, the twisted *anti* conformation of A molecule in Form II has intramolecular energy of 18 kJ·mol^{-1}, and the twisted *syn-anti* conformation of Form I has intramolecular energy of 15 kJ·mol^{-1}. Therefore, the intramolecular energy of Form II is lower by 9 kJ·mol^{-1}.

For the calculation of intermolecular energy, the crystal structure of Form I in the monoclinic *Pc* space group without disorder in the dimers formed by the *syn-anti*-conformers was used. Therefore, the lattice energy calculations are somewhat approximate and can have some deviations because of the lower symmetry used. Based on the obtained results, Form I has 8.5 kJ·mol^{-1} lower intermolecular energy than Form II (see Table 2). Therefore, the lattice energy of both polymorphs is almost identical, with that of Form II being calculated as 0.7 kJ·mol^{-1} lower, corresponding to the typical energy difference (<5 kJ·mol^{-1}) of organic polymorphs [61,66]. Although the calculated relative energy contradicts Form I being determined as the thermodynamically stable polymorph, the possibility for different

hydrogen atom arrangement in dimers could provide an entropy increase, resulting in lowering of the free energy of Form I.

Table 2. Selected crystallographic data and the calculated intramolecular, intermolecular, and lattice energies of MPBA polymorphs.

Polymorph	Form I	Form II
CSD Ref. code	UJACIT01 (original $P\overline{4}n2$ structure)	UJACIT
Z/Z'	4/0.5 (for $P\overline{4}n2$ structure) 4/2 (for Pc structure)	12/1.5
E_{intra}, kJ·mol^{-1}	15.2	6.0
E_{inter}, kJ·mol^{-1}	−144.4	−135.9
$(E_{ele} + E_{pol})/E_{disp}$	1.3	1.0
$E_{lattice}$, kJ·mol^{-1}	−129.2	−129.8

The pronounced differences in the hydrogen bonding in both polymorphs, as described above, result in high differences in the lattice energy component contributions and energy frameworks of both forms. As shown in Table 2, the electrostatic energy in Form I is the dominant component of the lattice energy, which can be associated with the extensive strong hydrogen bond network in this structure. Interestingly, despite the presence of hydrogen bonded chains in the structure of Form I, the electrostatic (Coulomb) energy (see Figure 7) is dominated by the interactions between the molecules that form the homodimers in the *bc* plane, while the interactions between the adjacent dimers in adjacent layers are notably less efficient. The strongest dispersion energy is observed between two molecules forming a $CH_3 \cdots \pi$ interaction along the *a*-axis. In contrast, the electrostatic energy and dispersion energy in Form II have a very similar contribution in the lattice energy, because of a much smaller amount of intermolecular hydrogen bonds and higher importance of the aromatic interactions, including $\pi \cdots \pi$ stacking. This is also observed in the electrostatic energy framework of Form II, as the strongest interactions observed between the molecules in the trimer are still notably less efficient than those in Form I. However, in this structure there are several molecule pairs with efficient dispersion energy in a different spatial arrangement, with the strongest dispersion interactions observed between the adjacent B molecules connected in a shifted $\pi \cdots \pi$ stacking manner and forming the hydrogen bonded trimers in a perpendicular direction. To sum up, despite overall more efficient dispersion interactions in Form II, the notably stronger hydrogen bonds in Form I are the reason for the higher intermolecular energy of this form, which could also explain its higher stability. The ability of hydrogen bonding to provide stabilization of the crystal structure has been shown before, e.g., in studies of proteins [67,68] and ritonavir [69].

Differences in the intermolecular interactions of both forms can also clearly be seen on the Hirshfeld surfaces and in the analysis of their 2D fingerprint plots (see Figure 8). As could be expected from the artificially decreased symmetry, both *symmetry independent* molecules of the structure in the *Pc* space group have identical 2D fingerprint plots with hydrogen bonds forming the boronic acid dimers and chains, and different -H $\cdots$ C- and -C $\cdots$ H- interactions (particularly from $CH_3 \cdots \pi$ interactions) being the main observable interactions. Logically, both molecules (A and B) of Form II had different Hirshfeld surfaces and their 2D fingerprint plots. Both molecules A and B have only one sharp peak corresponding to being a donor (A) or acceptor (B) of the strong intermolecular hydrogen bond, as can be seen in the fingerprint plots. Also, interactions associated with $\pi \cdots \pi$ stacking are present for molecule B, as also demonstrated by the energy framework diagrams of this polymorph.

3.5. Use of Full Interaction Maps to Understand Polymorph Stability and Effect of Crystallization Additives

The Full Interaction Map (FIM) visualizes regions around the molecule where, based on pre-extracted *IsoStar* interaction data from the CSD [52], intermolecular interactions are expected, allowing to evaluate whether interaction preferences within the lattice are satisfied.

FIM analysis has been shown to allow prediction of the stability of polymorphs [61,70,71]. Moreover, we speculate that if in a structure there are regions of the molecule in which the crystal lattice interactions are not satisfied, the additional interactions provided by the additives may stabilize the respective polymorph.
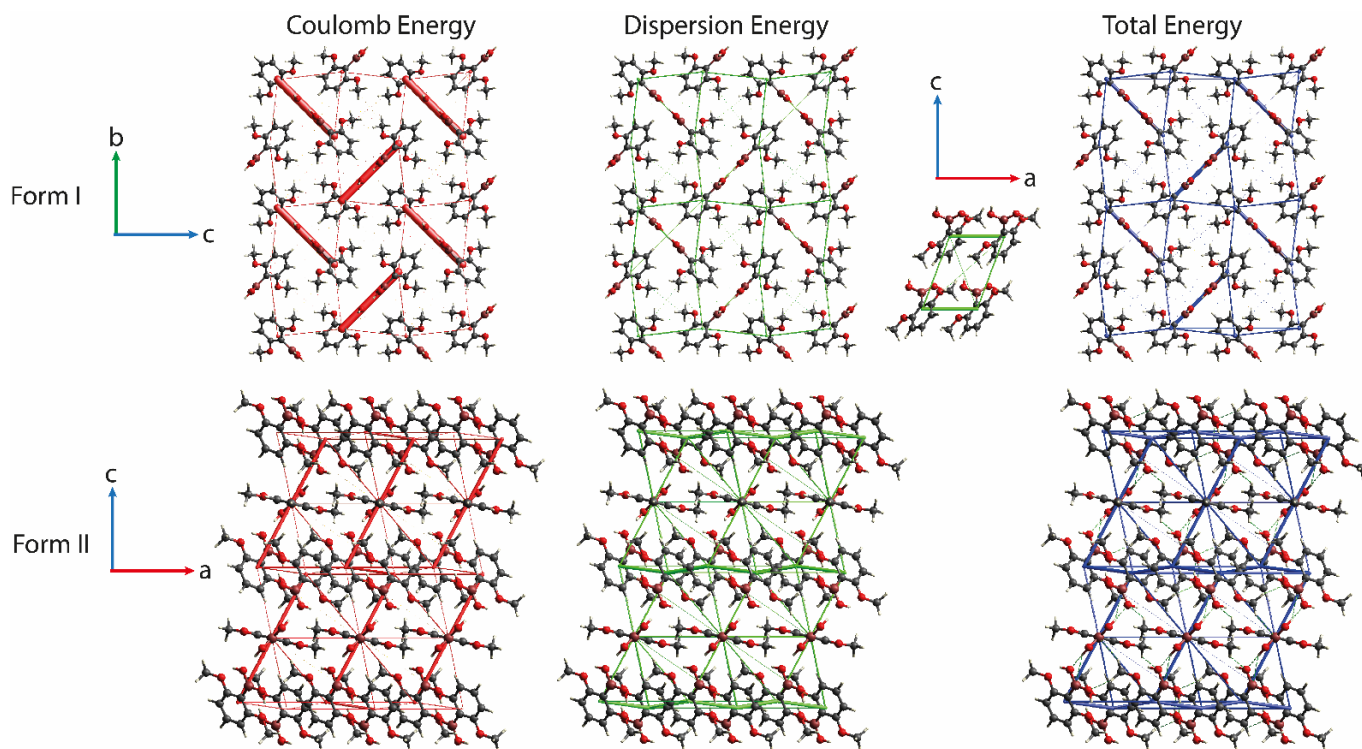

Figure 7. Energy-framework diagrams for E_{Coul}, E_{dis} and E_{tot} for MPBA Forms I and II. All images have the same tube size.
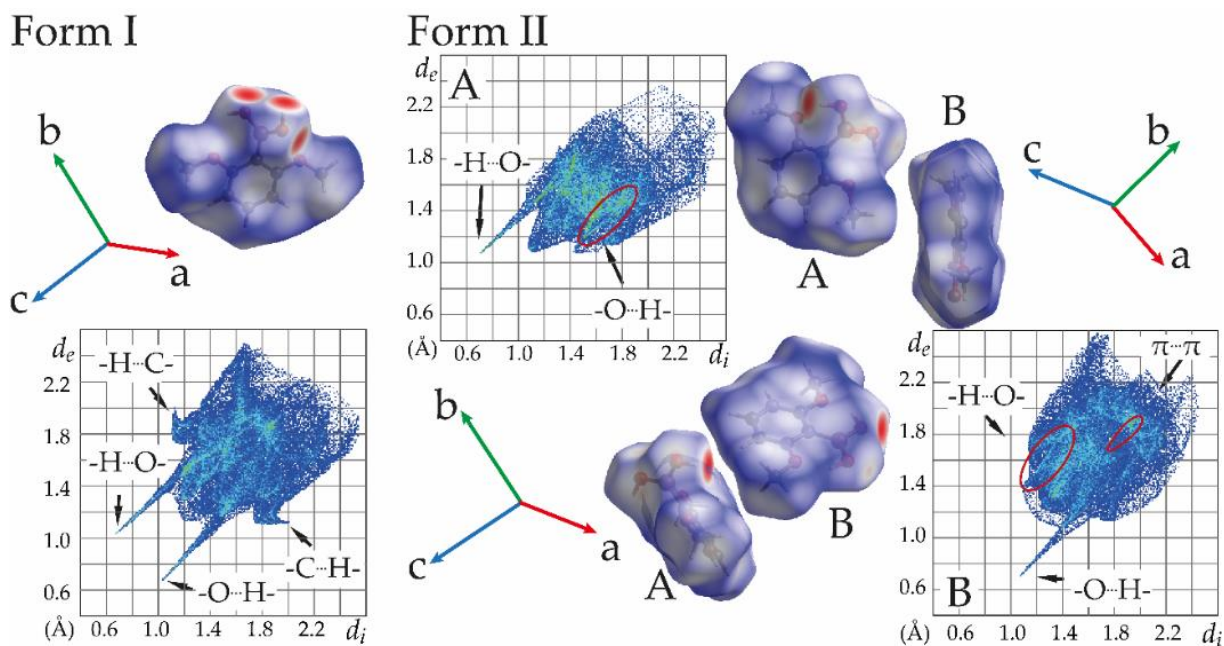

Figure 8. Hirshfeld surfaces and their 2D fingerprinting plots of MPBA Forms I and II. In the labels, the atom on the left is inside the Hirshfeld surface.

FIM analysis was performed for the original disordered Form I structure in the $P\bar{4}n2$ space group and for this polymorph with removed disorder in the Pc space group. Nearly identical FIMs were obtained for both symmetry independent molecules of the Pc structure, and they were highly similar to FIMs of this polymorph in the $P\bar{4}n2$ space group (except that the hydrogen bond donor and acceptor sites in dimer were discriminated) (see Figure 9). The MPBA molecule has two hydroxyl groups able to act as both hydrogen bond acceptors and donors. In the homodimers as in Form I, most of the interaction preferences are satisfied. Both hydrogen bond donors and acceptor sites in the boronic acid group are involved in dimer formation and hydrogen bonding between the dimers. Apart from this, both methoxy groups are potential hydrogen bond acceptors, and there is a preference for the involvement of aromatic C-H in weak hydrogen bonds or aromatic interactions and also a preference for aromatic π electrons to be involved in some interactions. These preferences are partly fulfilled by formation of weak hydrogen bonds, $CH_3 \cdots \pi$ interactions, and other aromatic interactions. In contrast, only half of the interaction preferences for hydrogen bonding are satisfied in Form II (see Figure 9). According to the FIM, the boronic acid group of molecule A prefers to be involved as the hydrogen bond acceptor with two donors, but instead only weak hydrogen bonds with the benzene C–H and methoxy groups (with $C \cdots O$ distance of 3.55 Å and 3.58 Å, respectively) are formed. There is an identical preference also for molecule B, and it is fulfilled for one of the oxygen atoms by the hydrogen bond O_A-$H \cdots O_B$, but the second oxygen atom forms a weak hydrogen bond with a methoxy group ($C \cdots O$ distance 3.32 Å). Therefore, the hydrogen bonding in Form II does not match the interaction preferences as in the CSD, and the three unsatisfied hydrogen bond acceptors may be the reason for the low stability of Form II and formation of this polymorph only under specific conditions. All the hydrogen bond donor capabilities in Form II, however, are satisfied by two O_A-$H \cdots O_B$ bonds for molecule A and the intramolecular hydrogen bonds for molecule B.
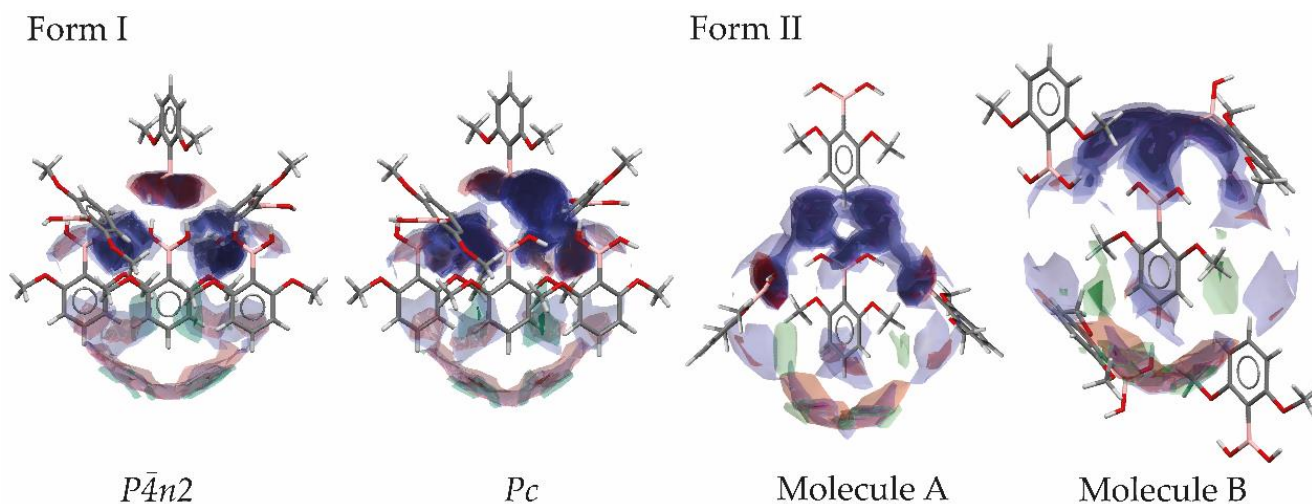

Figure 9. FIMs for MPBA polymorphs. Regions of hydrogen bond donor probability are shown in blue, hydrogen bond acceptors are shown in red, and hydrophobic interactions are shown in green.

If the morphology generated from the Form I structure in the $P\bar{4}n2$ and Pc space groups are compared, the effects of disorder in the $P\bar{4}n2$ structure and the lower symmetry of the Pc structure are visible. Because of the symmetry generated redundant hydrogen atoms in the disordered structure, FIMs on the $P\bar{4}n2$ Form I crystal have a larger hydrogen bond donor probability than on the Pc Form I crystal facets, which have a larger hydrogen bond acceptor probability (see Figure S9). Nevertheless, we analyse FIMs on $P\bar{4}n2$ morphology due to the loss of crystal symmetry in the Pc space group.

Overall, there are large differences between both polymorphs when FIMs on crystal facets are compared (see Figure 10). Form I crystals have a larger probability of being

involved in hydrophobic interactions (green) and interact with hydrogen bond acceptors (red) when compared to Form II. The largest facets {110} of Form I (space group $P\bar{4}n2$) have exposed benzene rings and grow through interactions with the benzene ring. The benzene rings on these facets can act as weak hydrogen bond acceptors (blue colour). This facet also grows by formation of dimers and requires attachment of a hydrogen bond acceptor such as oxygen (red colour). Smaller facets {101} and {10$\bar{1}$} of Form I are growing by formation of dimer chains; therefore, the probability of interacting with hydrogen bond donors (blue colour) is higher for these facets.
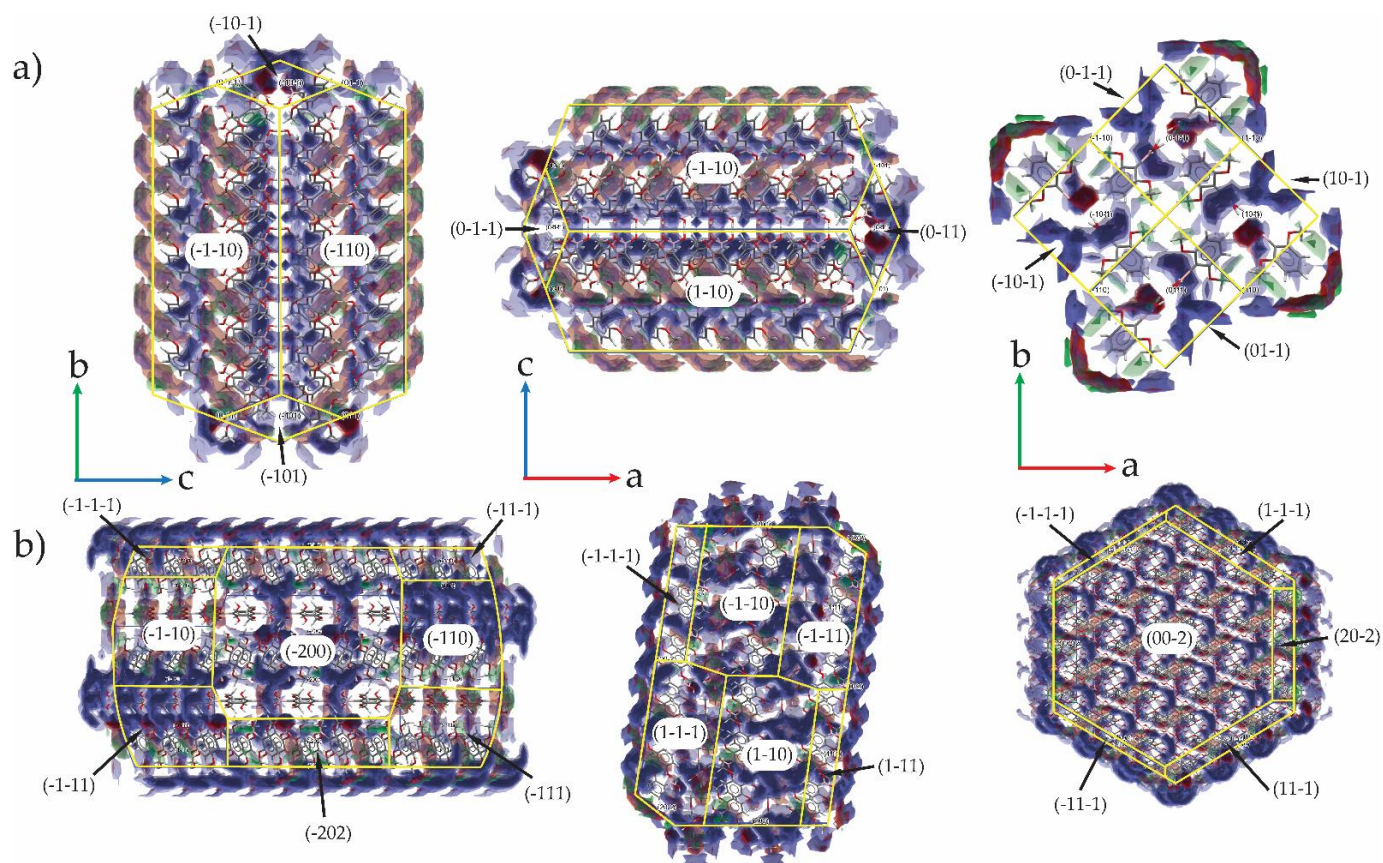

Figure 10. FIMs combined on the BFDH morphology of MPBA Form I (**a**) and Form II (**b**). Regions of hydrogen bond donor probability are shown in blue, hydrogen bond acceptors are shown in red, and hydrophobic interactions are shown in green.

The Form II crystal has a larger probability of interacting with hydrogen bond donors on the largest facets when compared to Form I (see the increase in blue coloured regions in Figure 10). On the largest edges {002} and {110} of Form II, in contrast to Form I, many hydrogen bond acceptor groups are exposed. On these facets, the oxygen atoms of the boronic acid groups in *anti*-planar conformation are forming hydrogen bonds and are growing by formation of trimers, so hydrogen bond acceptors are exposed and there is a great propensity to interact with hydrogen bond donors by these facets. Therefore, surfactants can interact as hydrogen bond donors with these facets more easily if compared to Form I, for which hydrogen bond acceptor groups cover a smaller area. The interactions between the crystals and additives could be similar to those Kim et al. [17] demonstrated between the crystals of hexahydro-1,3,5-trinitro-1,3,5-triazine (RDX) and amphiphilic additives using molecular simulations. Span 20 and OGP both have hydrogen bond donors (three and four, respectively) that can interact with the boronic acid group of MPBA and stabilize Form II crystals. Additionally, the hydrophobic site of the surfactants can decelerate phase transition by forming micelles or hemispheres and therefore prevent the reorganization

of molecules required for the transformation of Form II to Form I. This can also explain the small crystal size of Form II obtained in the experiments using these surfactants. It is possible that the hydrophobic part of the surfactants in surfactant micelles or hemispheres could inhibit crystal growth by steric effects preventing attachment of new growth units to the crystal facets.

4. Conclusions

Our studies of MPBA demonstrated that Form I is obtained in evaporation crystallization from most solvents and cooling crystallization from almost all the tested solvents. However, evaporation crystallization from alcohols produced Form II, and evaporation of an isopropanol solution produced the new polymorph Form III. Thermal characterization showed that Form I is the most stable polymorph and that both Form II and Form III are monotropically related to Form I. We observed that Form II and Form III are unstable—Form II transformed to Form I in <24 h, whereas Form III transformed to Form II in <1 h.

The MPBA molecule in planar *anti* conformation is the most stable conformer as shown in the ab initio calculations. Therefore, Form II has lower intramolecular energy. However, Form I has lower intermolecular energy, and its structure is mostly stabilized by the electrostatic energy of strong hydrogen bonds, whereas in Form II the electrostatic and dispersion energy contributions are almost equal, partly because of the less efficient hydrogen bonding. Nevertheless, the lattice energy obtained as sum of the intra- and intermolecular energy of Form II is slightly lower.

More extensive exploration of the crystallization from toluene and water showed that the cooling rate and supersaturation do not affect the crystallization polymorphic outcome. By performing crystallizations in the presence of additives, we found that Span 20 and OGP provide crystallization of the metastable forms in evaporation crystallization at 50 °C. We also showed that the solvent does not play any role in regulating the crystallization outcome in the presence of Span 20 under these conditions, as crystallization is actually occurring from a MPBA solution in liquid Span 20. Moreover, OGP and Span 20 stabilize Form II for up to 1 month at ambient temperature. Although Span 20 also allowed for the crystallization of Form III, this form was not stabilized by Span 20. We showed that not every viscous liquid allows crystallization of the metastable forms because, among several other viscous additives tested, only PEG 600 facilitated crystallization of Form II.

We propose that Span 20 and OGP provide crystallization and stabilization of Form II by intermolecular interactions. On the crystal edges of Form I, mostly atoms keen to form hydrophobic interactions and hydrogen bond donors (boronic acid groups and benzene rings) are exposed, whereas the edges of Form II can interact with hydrogen bond donors because of the many exposed hydrogen bond acceptor groups (boronic acid oxygen atoms). Furthermore, for Form II, the FIM regions where interactions with hydrogen bond donors are likely to occur are larger and more sterically available than for Form I. Although many of the tested additives are hydrogen bond donors, only Span 20 and OGP efficiently interacted with MPBA and provided crystallization of Form II. It is possible that the hydrogen bond donor groups interact with Form II crystal edges, but hydrophobic parts of these additives decelerate the phase transition and provide the stabilization of this polymorph.

Supplementary Materials: The following supporting information can be downloaded at: https://www.mdpi.com/article/10.3390/cryst12121738/s1, Table S1: List of additives used in the study; Table S2: Approximate solubility of MPBA Form I in different solvents; Figure S1: CSD search results for phenylboronic acid derivatives; Figure S2: Types of dimeric hydrogen bond motifs observed in the crystal structures of phenylboronic acid derivatives in CSD; Figure S3: Types of non-dimeric hydrogen bond motifs observed in the crystal structures of phenylboronic acid derivatives in CSD; Table S3: Polymorphism observed in phenylboronic acid derivatives; Table S4: Types of dimeric structures from CSD search results for phenylboronic acid derivatives; Table S5: Types of non-dimeric structures from the CSD search results for phenylboronic acid derivatives; Figure S4: Hydrogen bonding phenylboronic acid derivative structures containing chains and dimers; Figure S5: DSC/TG curves of MPBA Form I; Figure S6: DSC/TG curves of MPBA Form II; Figure S7: DSC/TG curves of

MPBA Form III; Figure S8: Results of the crystallization in the presence of additives from toluene and water; Table S6: Intramolecular energies and torsion angle data of MPBA polymorphs; Figure S9: FIMs combined on the BFDH morphology of MPBA polymorph I using different crystal structure models.

Author Contributions: Investigation, writing—original draft preparation and visualization, A.S.; Conceptualization, methodology, and writing—review and editing, A.S. and A.B.; Supervision, A.B. All authors have read and agreed to the published version of the manuscript.

Data Availability Statement: No new data were created or analyzed in this study. Data sharing is not applicable to this article.

Conflicts of Interest: The authors declare that they have no conflict of interest.

References

1. Hilfiker, R. (Ed.) *Polymorphism: In the Pharmaceutical Industry*; Wiley-VCH Verlag GmbH & Co. KGaA: Weinheim, Germany, 2006; ISBN 9783527311460.
2. Aitipamula, S.; Nangia, A. Polymorphism: Fundamentals and Applications. In *Supramolecular Chemistry*; John Wiley & Sons, Ltd.: Chichester, UK, 2012; ISBN 9780470661345.
3. Lu, J.; Rohani, S. Polymorphism and Crystallization of Active Pharmaceutical Ingredients (APIs). *Curr. Med. Chem.* **2009**, *16*, 884–905. [CrossRef] [PubMed]
4. Lee, E.H. A Practical Guide to Pharmaceutical Polymorph Screening & Selection. *Asian J. Pharm. Sci.* **2014**, *9*, 163–175. [CrossRef]
5. Pudipeddi, M.; Serajuddin, A.T.M. Trends in Solubility of Polymorphs. *J. Pharm. Sci.* **2005**, *94*, 929–939. [CrossRef] [PubMed]
6. Nicoud, L.; Licordari, F.; Myerson, A.S. Estimation of the Solubility of Metastable Polymorphs: A Critical Review. *Cryst. Growth Des.* **2018**, *18*, 7228–7237. [CrossRef]
7. Censi, R.; di Martino, P. Polymorph Impact on the Bioavailability and Stability of Poorly Soluble Drugs. *Molecules* **2015**, *20*, 18759–18776. [CrossRef]
8. Nogueira, B.A.; Castiglioni, C.; Fausto, R. Color Polymorphism in Organic Crystals. *Commun. Chem.* **2020**, *3*, 34. [CrossRef]
9. Neumann, M.A.; van de Streek, J. How Many Ritonavir Cases Are There Still out There? *Faraday Discuss.* **2018**, *211*, 441–458. [CrossRef]
10. European Medicines Agency Public Statement: Suply of Norvir Hard Capsules. Available online: https://www.ema.europa.eu/en/documents/public-statement/public-statement-supply-norvir-hard-capsules_en.pdf (accessed on 30 January 2022).
11. Xu, S.; Cao, D.; Liu, Y.; Wang, Y. Role of Additives in Crystal Nucleation from Solutions: A Review. *Cryst. Growth Des.* **2021**, *22*, 2001–2022. [CrossRef]
12. Kras, W.; Carletta, A.; Montis, R.; Sullivan, R.A.; Cruz-Cabeza, A.J. Switching Polymorph Stabilities with Impurities Provides a Thermodynamic Route to Benzamide Form III. *Commun. Chem.* **2021**, *4*, 38. [CrossRef]
13. Bērziņš, A.; Trimdale-Deksne, A.; Belyakov, S.; ter Horst, J.H. Reversing the Polymorphic Outcome of Crystallization and the Apparent Relative Stability of Nitrofurantoin Polymorphs Using Additives, University of Latvia, Faculty of Chemistry, Riga, Latvia. 2022, *manuscript in preparation; to be submitted*.
14. Poornachary, S.K.; Han, G.; Kwek, J.W.; Chow, P.S.; Tan, R.B.H. Crystallizing Micronized Particles of a Poorly Water-Soluble Active Pharmaceutical Ingredient: Nucleation Enhancement by Polymeric Additives. *Cryst. Growth Des.* **2016**, *16*, 749–758. [CrossRef]
15. Wu, H.; Wang, J.; Liu, Q.; Zong, S.; Tian, B.; Huang, X.; Wang, T.; Yin, Q.; Hao, H. Influences and the Mechanism of Additives on Intensifying Nucleation and Growth of P-Methylacetanilide. *Cryst. Growth Des.* **2020**, *20*, 973–983. [CrossRef]
16. Quan, Y.; Yang, Y.; Xu, S.; Zhu, P.; Liu, S.; Jia, L.; Gong, J. Insight into the Role of Piperazine in the Thermodynamics and Nucleation Kinetics of the Triethylenediamine-Methyl Tertiary Butyl Ether System. *CrystEngComm* **2019**, *21*, 948–956. [CrossRef]
17. Kim, J.W.; Park, J.H.; Shim, H.M.; Koo, K.K. Effect of Amphiphilic Additives on Nucleation of Hexahydro-1,3,5-Trinitro-1,3,5-Triazine. *Cryst. Growth Des.* **2013**, *13*, 4688–4694. [CrossRef]
18. Pino-García, O.; Rasmuson, Å.C. Influence of Additives on Nucleation of Vanillin: Experiments and Introductory Molecular Simulations. *Cryst. Growth Des.* **2004**, *4*, 1025–1037. [CrossRef]
19. Poon, G.G.; Seritan, S.; Peters, B. A Design Equation for Low Dosage Additives That Accelerate Nucleation. *Faraday Discuss.* **2015**, *179*, 329–341. [CrossRef]
20. Lin, J.; Shi, P.; Wang, Y.; Wang, L.; Ma, Y.; Liu, F.; Wu, S.; Gong, J. Template Design Based on Molecular and Crystal Structure Similarity to Regulate Conformational Polymorphism Nucleation: The Case of α,ω-Alkanedicarboxylic Acids. *IUCrJ* **2021**, *8*, 814–822. [CrossRef]
21. Singh, M.K. Controlling the Aqueous Growth of Urea Crystals with Different Growth Inhibitors: A Molecular-Scale Study. *RSC Adv.* **2021**, *11*, 12938–12950. [CrossRef]

22. Simone, E.; Steele, G.; Nagy, Z.K. Tailoring Crystal Shape and Polymorphism Using Combinations of Solvents and a Structurally Related Additive. *CrystEngComm* **2015**, *17*, 9370–9379. [CrossRef]

23. Urwin, S.J.; Yerdelen, S.; Houson, I.; ter Horst, J.H. Impact of Impurities on Crystallization and Product Quality: A Case Study with Paracetamol. *Crystals* **2021**, *11*, 1344. [CrossRef]

24. Agnew, L.R.; Cruickshank, D.L.; McGlone, T.; Wilson, C.C. Controlled Production of the Elusive Metastable Form II of Acetaminophen (Paracetamol): A Fully Scalable Templating Approach in a Cooling Environment. *ChemComm* **2016**, *52*, 7368–7371. [CrossRef]

25. Shi, P.; Xu, S.; Yang, H.; Wu, S.; Tang, W.; Wang, J.; Gong, J. Use of Additives to Regulate Solute Aggregation and Direct Conformational Polymorph Nucleation of Pimelic Acid. *IUCrJ* **2021**, *8*, 161–167. [CrossRef] [PubMed]

26. European Medicines Agency. Council of Europe Control of Impurities in Substances for Pharmaceutical Use. In *European Pharmacopoeia, Supplement 10.8*; European Medicines Agency: Strasbourg, France, 2022; pp. 763–765.

27. Giordani, C.F.A.; Campanharo, S.; Wingert, N.R.; Bueno, L.M.; Manoel, J.W.; Costa, B.; Cattani, S.; Arbo, M.D.; Garcia, S.C.; Garcia, C.V.; et al. In Vitro Toxic Evaluation of Two Gliptins and Their Main Impurities of Synthesis. *BMC Pharmacol. Toxicol.* **2019**, *20*, 1–9. [CrossRef] [PubMed]

28. Prajapati, P.; Agrawal, Y.K. Analysis and Impurity Identification in Pharmaceuticals. *Rev. Anal. Chem.* **2014**, *33*, 123–133. [CrossRef]

29. Abdin, A.Y.; Yeboah, P.; Jacob, C. Chemical Impurities: An Epistemological Riddle with Serious Side Effects. *Int. J. Environ. Res. Public Health* **2020**, *17*, 1030. [CrossRef]

30. Smith, S.W. Chiral Toxicology: It's the Same Thing . . . Only Different. *Toxicol. Sci.* **2009**, *110*, 4–30. [CrossRef]

31. Sinko, P.J. Pharmaceutical Polymers. In *Martin's Physical Pharmacy and Pharmaceutical Sciences*; Troy, D.B., Ed.; Wolters Kluwer, Lippincott Williams & Wilkins: Philadelphia, PA, USA, 2016; pp. 508–514, ISBN 9781451191455.

32. Tadros, T.F. Surfactants in Pharmaceutical Formulations. In *Applied Surfactants: Principles and Applications*; Wiley-VCH: Weinheim, Germany, 2005; pp. 433–501. ISBN 9783527306299.

33. Tadros, T.F. Surfactants, Industrial Applications. In *Encyclopedia of Physical Science Technology*, 3rd ed.; Meyers, R.A., Ed.; Academic Press: Cambridge, MA, USA, 2003; Volume 16, pp. 423–438, ISBN 9780122274107. [CrossRef]

34. Garti, N.; Zour, H. The Effect of Surfactants on the Crystallization and Polymorphic Transformation of Glutamic Acid. *J. Cryst. Growth* **1997**, *172*, 486–498. [CrossRef]

35. Feng, Y.; Meng, Y.; Tan, F.; Lv, L.; Li, Z.; Wang, Y.; Yang, Y.; Gong, W.; Yang, M. Effect of Surfactants and Polymers on the Dissolution Behavior of Supersaturable Tecovirimat-4-Hydroxybenzoic Acid Cocrystals. *Pharmaceutics* **2021**, *13*, 1772. [CrossRef]

36. Cyrański, M.K.; Klimentowska, P.; Rydzewska, A.; Serwatowski, J.; Sporzyński, A.; Stępień, D.K. Towards a Monomeric Structure of Phenylboronic Acid: The Influence of Ortho-Alkoxy Substituents on the Crystal Structure. *CrystEngComm* **2012**, *14*, 6282–6294. [CrossRef]

37. Adamczyk-Woźniak, A.; Gozdalik, J.T.; Kaczorowska, E.; Durka, K.; Wieczorek, D.; Zarzeczańska, D.; Sporzyński, A. (Trifluoromethoxy)Phenylboronic Acids: Structures, Properties, and Antibacterial Activity. *Molecules* **2021**, *26*, 2007. [CrossRef]

38. Adamczyk-Woźniak, A.; Gozdalik, J.T.; Wieczorek, D.; Madura, I.D.; Kaczorowska, E.; Brzezińska, E.; Sporzyński, A.; Lipok, J. Synthesis, Properties and Antimicrobial Activity of 5-Trifluoromethyl-2-Formylphenylboronic Acid. *Molecules* **2020**, *25*, 799. [CrossRef] [PubMed]

39. Borys, K.M.; Wieczorek, D.; Pecura, K.; Lipok, J.; Adamczyk-Woźniak, A. Antifungal Activity and Tautomeric Cyclization Equilibria of Formylphenylboronic Acids. *Bioorg. Chem.* **2019**, *91*, 103081. [CrossRef] [PubMed]

40. Hiller, N.D.J.; do Amaral e Silva, N.A.; Tavares, T.A.; Faria, R.X.; Eberlin, M.N.; de Luna Martins, D. Arylboronic Acids and Their Myriad of Applications Beyond Organic Synthesis. *Eur. J. Org. Chem.* **2020**, *2020*, 4841–4877. [CrossRef]

41. Cruz, C.D.; Wrigstedt, P.; Moslova, K.; Iashin, V.; Mäkkylä, H.; Ghemtio, L.; Heikkinen, S.; Tammela, P.; Perea-Buceta, J.E. Installation of an Aryl Boronic Acid Function into the External Section of -Aryl-Oxazolidinones: Synthesis and Antimicrobial Evaluation. *Eur. J. Med. Chem.* **2021**, *211*, 113002. [CrossRef]

42. Silva, M.P.; Saraiva, L.; Pinto, M.; Sousa, M.E. Boronic Acids and Their Derivatives in Medicinal Chemistry: Synthesis and Biological Applications. *Molecules* **2020**, *25*, 4323. [CrossRef]

43. Groom, C.R.; Bruno, I.J.; Lightfoot, M.P.; Ward, S.C. The Cambridge Structural Database. *Acta Crystallogr. B Struct. Sci. Cryst. Eng. Mater.* **2016**, *72*, 171–179. [CrossRef] [PubMed]

44. Bruno, I.J.; Cole, J.C.; Edgington, P.R.; Kessler, M.; Macrae, C.F.; McCabe, P.; Pearson, J.; Taylor, R. New Software for Searching the Cambridge Structural Database and Visualizing Crystal Structures. *Acta Crystallogr. B* **2002**, *58*, 389–397. [CrossRef] [PubMed]

45. Macrae, C.F.; Sovago, I.; Cottrell, S.J.; Galek, P.T.A.; McCabe, P.; Pidcock, E.; Platings, M.; Shields, G.P.; Stevens, J.S.; Towler, M.; et al. Mercury 4.0: From Visualization to Analysis, Design and Prediction. *J. Appl. Crystallogr.* **2020**, *53*, 226–235. [CrossRef]

46. Giannozzi, P.; Baroni, S.; Bonini, N.; Calandra, M.; Car, R.; Cavazzoni, C.; Ceresoli, D.; Chiarotti, G.L.; Cococcioni, M.; Dabo, I.; et al. QUANTUM ESPRESSO: A Modular and Open-Source Software Project for Quantum Simulations of Materials. *J. Phys. Condens. Matter* **2009**, *21*, 395502. [CrossRef]

47. Stokes, H.T.; Hatch, D.M.; Campbell, B.J. ISOCIF, ISOTROPY Software Suite, Department of Physics and Astronomy, Brigham Young University, Provo, Utah, 84602, USA. 2022. Available online: iso.byu.edu/iso/isocif.php (accessed on 21 June 2022).

48. Grimme, S.; Antony, J.; Ehrlich, S.; Krieg, H. A Consistent and Accurate Ab Initio Parametrization of Density Functional Dispersion Correction (DFT-D) for the 94 Elements H-Pu. *J. Chem. Phys.* **2010**, *132*, 154104. [CrossRef]

49. Spackman, P.R.; Turner, M.J.; McKinnon, J.J.; Wolff, S.K.; Grimwood, D.J.; Jayatilaka, D.; Spackman, M.A. CrystalExplorer: A Program for Hirshfeld Surface Analysis, Visualization and Quantitative Analysis of Molecular Crystals. *J. Appl. Crystallogr.* **2021**, *54*, 1006–1011. [CrossRef]

50. Frisch, J.; Trucks, G.W.; Schlegel, H.B.; Scuseria, G.E.; Robb, M.A.; Cheeseman, J.R.; Scalmani, G.; Barone, V.; Petersson, G.A.; Nakatsuji, H.; et al. *Gaussian 09W, Revision D.01*; Gaussian, Inc.: Wallingford, CT, USA, 2016.

51. Karamertzanis, P.G.; Day, G.M.; Welch, G.W.A.; Kendrick, J.; Leusen, F.J.J.; Neumann, M.A.; Price, S.L. Modeling the Interplay of Inter- and Intramolecular Hydrogen Bonding in Conformational Polymorphs. *J. Chem. Phys.* **2008**, *128*, 244708. [CrossRef] [PubMed]

52. Wood, P.A.; Olsson, T.S.G.; Cole, J.C.; Cottrell, S.J.; Feeder, N.; Galek, P.T.A.; Groom, C.R.; Pidcock, E. Evaluation of Molecular Crystal Structures Using Full Interaction Maps. *CrystEngComm* **2013**, *15*, 65–72. [CrossRef]

53. Ouyang, J.; Xing, X.; Chen, J.; Zhou, L.; Liu, Z.; Heng, J.Y.Y. Effects of Solvent, Supersaturation Ratio and Silica Template on Morphology and Polymorph Evolution of Vanillin during Swift Cooling Crystallization. *Particuology* **2022**, *65*, 93–104. [CrossRef]

54. Ouyang, J.; Chen, J.; Rosbottom, I.; Chen, W.; Guo, M.; Heng, J.Y.Y. Supersaturation and Solvent Dependent Nucleation of Carbamazepine Polymorphs during Rapid Cooling Crystallization. *CrystEngComm* **2021**, *23*, 813–823. [CrossRef]

55. Datta, S.; Grant, D.J.W. Effect of Supersaturation on the Crystallization of Phenylbutazone Polymorphs. *Cryst. Res. Technol.* **2005**, *40*, 233–242. [CrossRef]

56. Bemisderfer, K.; Nazarenko, A.Y. Two Forms of (Naphthalen-1-Yl)Boronic Acid. *Acta Crystallogr. E Crystallogr. Commun.* **2016**, *72*, 1285–1289. [CrossRef] [PubMed]

57. Dąbrowski, M.; Durka, K.; Luliński, S.; Serwatowski, J. (2,4-Dipropoxyphenyl)Boronic Acid. *Acta Crystallogr. Sect. E Struct. Rep. Online* **2011**, *67*, o3455. [CrossRef]

58. Bai, S.Z.; Lou, X.H.; Li, H.M.; Yang, W.C.; Shi, H. Refinement of Crystal Structure of 2-Biphenylboronic Acid, $C_{12}H_{11}BO_2$. *Z. Krist.-New Cryst. Struct.* **2010**, *225*, 295–296. [CrossRef]

59. Durka, K.; Kliś, T.; Serwatowski, J. Crystal Structure of (2-Benzyloxypyrimidin-5-Yl)Boronic Acid. *Acta Crystallogr. Sect. E Struct. Rep. Online* **2014**, *70*, o1259–o1260. [CrossRef]

60. Cárdenas-Valenzuela, A.J.; González-García, G.; Zárraga-Nuñez, R.; Höpfl, H.; Campos-Gaxiola, J.J.; Cruz-Enríquez, A. Crystal Structure and Hirshfeld Surface Analysis of 3-Cyanophenylboronic Acid. *Acta Crystallogr. E Crystallogr. Commun.* **2018**, *74*, 441–444. [CrossRef]

61. Cruz-Cabeza, A.J.; Reutzel-Edens, S.M.; Bernstein, J. Facts and Fictions about Polymorphism. *Chem. Soc. Rev.* **2015**, *44*, 8619–8635. [CrossRef]

62. Burger, A.; Ramberger, R. On the Polymorphism of Pharmaceuticals and Other Molecular Crystals. I. *Mikrochim. Acta* **1979**, *72*, 259–271. [CrossRef]

63. Rietveld, I.B.; Barrio, M.; Lloveras, P.; Céolin, R.; Tamarit, J.-L. Polymorphism of Spironolactone: An Unprecedented Case of Monotropy Turning to Enantiotropy with a Huge Difference in the Melting Temperatures. *Int. J. Pharm.* **2018**, *552*, 193–205. [CrossRef] [PubMed]

64. Semjonova, A.; Bērziņš, A. Controlling the Polymorphic Outcome of 2,6-Dimethoxybenzoic Acid Crystallization Using Additives. *Crystals* **2022**, *12*, 1161. [CrossRef]

65. Larkin, J.D.; Bhat, K.L.; Markham, G.D.; Brooks, B.R.; Schaefer, H.F.; Bock, C.W. Structure of the Boronic Acid Dimer and the Relative Stabilities of Its Conformers. *J. Phys. Chem. A* **2006**, *110*, 10633–10642. [CrossRef] [PubMed]

66. Nyman, J.; Day, G.M. Static and Lattice Vibrational Energy Differences between Polymorphs. *CrystEngComm* **2015**, *17*, 5154–5165. [CrossRef]

67. Takahashi, T.; Endo, S.; Nagayama, K. Stabilization of Protein Crystals by Electrostatic Interactions as Revealed by a Numerical Approach. *J. Mol. Biol.* **1993**, *234*, 421–432. [CrossRef]

68. Takahashi, T. Significant Role of Electrostatic Interactions for Stabilization of Protein Assemblies. *Adv. Biophys.* **1997**, *34*, 41–54. [CrossRef]

69. Wang, C.; Rosbottom, I.; Turner, T.D.; Laing, S.; Maloney, A.G.P.; Sheikh, A.Y.; Docherty, R.; Yin, Q.; Roberts, K.J. Molecular, Solid-State and Surface Structures of the Conformational Polymorphic Forms of Ritonavir in Relation to Their Physicochemical Properties. *Pharm. Res.* **2021**, *38*, 971–990. [CrossRef]

70. Taylor, R.; Wood, P.A. A Million Crystal Structures: The Whole Is Greater than the Sum of Its Parts. *Chem. Rev.* **2019**, *119*, 9427–9477. [CrossRef]

71. Feeder, N.; Pidcock, E.; Reilly, A.M.; Sadiq, G.; Doherty, C.L.; Back, K.R.; Meenan, P.; Docherty, R. The Integration of Solid-Form Informatics into Solid-Form Selection. *J. Pharm. Pharmacol.* **2015**, *67*, 857–868. [CrossRef] [PubMed]